Journal of Applied Physics

RESEARCH ARTICLE | AUGUST 08 2024

Comprehensive study of interface state via the time-dependent second harmonic generation

Libo Zhang; Li Ye ; Weiwei Zhao; Chongji Huang ; Tao Li ; Tai Min; Jinbo Yang ; Mingliang Tian ; Xuegang Chen

J. Appl. Phys. 136, 065301 (2024)
https://doi.org/10.1063/5.0188344

Journal of Applied Physics | ARTICLE | pubs.aip.org/aip/jap

Comprehensive study of interface state via the time-dependent second harmonic generation

Cite as: J. Appl. Phys. **136**, 065301 (2024); doi: 10.1063/5.0188344
Submitted: 21 November 2023 · Accepted: 25 July 2024 ·
Published Online: 8 August 2024

Libo Zhang,[1,2] Li Ye,[2] Weiwei Zhao,[3] Chongji Huang,[3] Tao Li,[4] Tai Min,[4] Jinbo Yang,[5] Mingliang Tian,[6,7] and Xuegang Chen[1,8,a)]

AFFILIATIONS

[1]Center of Free Electron Laser & High Magnetic Field, Institutes of Physical Science and Information Technology, Anhui University, Hefei 230601, China
[2]School of Materials Science and Engineering, Anhui University, Hefei 230601, China
[3]Shanghai Aspiring Semiconductor Equipment Co., Ltd and Aspiring Semiconductor (Beijing) Co., Ltd, Shanghai 200082, China
[4]Center for Spintronics and Quantum Systems, State Key Laboratory for Mechanical Behavior of Materials, Department of Materials Science and Engineering, Xi'an Jiaotong University, Xi'an, Shaanxi 710049, China
[5]State Key Laboratory for Mesoscopic Physics, School of Physics, Peking University, Beijing 100871, China
[6]School of Physics and Optoelectronic Engineering, Anhui University, Hefei 230601, China
[7]Anhui Province Key Laboratory of Condensed Matter Physics at Extreme Conditions, High Magnetic Field Laboratory, Chinese Academy of Sciences, Hefei 230031, China
[8]Information Materials and Intelligent Sensing Laboratory of Anhui Province, Anhui Key Laboratory of Magnetic Functional Materials and Devices, Anhui University, Hefei 230601, China

[a)]**Author to whom correspondence should be addressed:** xgchen@ahu.edu.cn

ABSTRACT

Electric field induced time-dependent second harmonic generation (TD-SHG) is an emerging sensitive and non-contact method for qualitatively/quantitatively probing semiconductor parameters. The TD-SHG signal is related to the evolution of the built-in electric field due to laser-induced electron generation and transportation. Here, we conducted a comprehensive study of fixed charge density (Q_{ox}) and interface state density (D_{it}) using the conventional conductance method to compare them with the SHG signal from TD-SHG. The extracted Q_{ox} is around 2.49×10^{10} cm^{-2} regardless of SiO_2 thickness, corresponding to the constant SHG intensity at the minimum of TD-SHG. The extracted D_{it} linearly decreases with the SiO_2 thickness, which is related to the linear change of extracted time constant from TD-SHG. Therefore, the TD-SHG, being a sensitive and non-contact method as well as simple and fast, can serve as an alternative approach to test the semiconductor parameters, which may facilitate semiconductor testing.

I. INTRODUCTION

As the size of silicon-based devices continues to shrink, it becomes a crucial issue to investigate interface properties of dielectric thin films, which can directly affect the device yield and performance.[1,2] The traditional electrical characterization methods, such as the voltage–capacitance method (C–V),[3] conductance method ($G/\omega - f$),[4,5] light-assisted method,[6,7] Terman method,[8] etc., require the metal electrodes from the standard lithography method, which needs considerable surface area for metal electrodes. Consequently, the tested sample cannot be used in device fabrication anymore. Recently, TD-SHG has emerged as a sensitive, non-contact probe for qualitatively estimating the semiconductor parameters, such as fixed charge density and interface state density. It can also be used to evaluate the dopant type and dopant density in the Si/SiO_2 systems.[9–12] Additionally, the TD-SHG technique can be used to estimate the band-offset[13] as well as the hot carrier injection in the silicon-on-insulator system,[14] which are the key

factors in determining the device performance. Therefore, an efficient method as well as a thorough understanding of collected data should be proposed to realize the sensitive and non-contact testing of silicon-based thin films and heterostructures.

Recently, the second harmonic generation (SHG) signal has been used to evaluate the symmetry of materials, especially in the systems with inverse symmetry breaking, such as ferroelectric materials.[15–17] With the development of the SHG technique, it has become a tool for noninvasively probing buried interfaces.[13,18,19] Mihaychuk and co-workers demonstrated that TD-SHG can be used to extract the interfacial information through analyzing the evolution of electric field induced second harmonic (EFISH) signal.[20] Subsequently, the TD-SHG was developed as a non-destructive and non-contact technique to measure the interfacial electric field using the following expression:[21–23]

$$I_{2\omega}(t) \propto |\chi^{(2)}_{\text{interface}} + \chi^{(3)}|[E_{\text{dc}} + E(t)]|^2 I^2_{\omega}. \quad (1)$$

Here, $I_{2\omega}(t)$, $\chi^2_{\text{interface}}$, χ^3, and I^2_{ω} are the intensity of SHG, the second-order nonlinear susceptibility at the interface, the third-order nonlinear susceptibility, and the intensity of the incident laser with the wavelength of ω, respectively.[9,11,24] E_{dc} is the initial build-in electric field at the interface ($t = 0$), which is mainly from the fixed charge of the oxide layer.[12] $E(t)$ is the interfacial electric field from the laser-induced electron/hole separation. Here, a connection between the evolution EFISH and the fixed charge density (Q_{ox}) of the dielectric layer is built, which allows for the evaluation of the interfacial electric field as well as the interface quality. Typically, the second-order susceptibility tensor of single crystal silicon is zero, contributing no SHG signal. However, when the dielectric layer is grown on silicon, forming a specific interface with a broken symmetry, the interfacial second-order susceptibility tensor contributes to the SHG signal.[25] Under laser irradiation, electrons in the valence band (VB) of the silicon substrate are excited to the SiO_2 conduction band (CB), thereby causing the electron/hole separation. Then, the electrons are transported/trapped at the interface or surface, corresponding to the TD-SHG signal.[10]

In this work, the TD-SHG method is used to characterize the interface state density (D_{it}) and fixed charge density (Q_{ox}) of the SiO_2/Si interface, which is compared with the traditional conductance method. We found that a minimum signal under a low laser power in EFISH is mainly related to Q_{ox}, while the time evolution of the SHG signal corresponds to D_{it}. The extracted Q_{ox} is around 2.49×10^{10} cm^{-2}, regardless of SiO_2 thickness, indicating a constant SHG intensity at the minimum of TD-SHG. The extracted D_{it} linearly decreases with the increasing SiO_2 thickness, which is related to the linear change of extracted time constant from TD-SHG. Accordingly, TD-SHG is a qualitative, sensitive, non-contact, and fast method to test the semiconductor parameters, potentially facilitating the semiconductor metrology.

II. EXPERIMENTAL DETAILS

SiO_2 thin films of various thicknesses (5–20 nm) were deposited on p-type Si substrates (carrier density of $\sim 4 \times 10^{17}$ cm^{-3}) via atomic layer deposition (ALD). The square metal electrodes [Ti (5 nm)/Au (80 nm)] with different pad sizes were prepared by conventional photolithography, followed by the e-beam evaporation process. The fabricated metal-oxide-semiconductor (MOS) structure is displayed in Fig. 1(a). The surface morphology of the SiO_2 film was characterized by atomic force microscopy (AFM, model AFM5500 M). The J–V characteristics were tested in a home-built setup with a Keithley 2636B source measure unit controlled by the Labview program. The C–V and $G/\omega - f$ measurements were carried out using a Keysight E4980A precision LCR meter. The positive voltage is always defined as a voltage applied on the top Au electrode. TD-SHG was performed using an Aspirer 3000 system with the laser of 780 nm (repetition frequency of 80 MHz and pulse width of 150 fs). The incident P-polarized laser (780 nm) illuminates the sample at 45°. The generated second harmonic signal ($\lambda = 390$ nm) was collected. All the measurements in our experiments were conducted at room temperature in a dark environment.

III. RESULTS AND DISCUSSION

The typical morphology of the as-grown SiO_2 film is characterized by atomic force microscopy ($2 \times 2\,\mu m^2$) as shown in Fig. 1(b). The AFM image reveals a flat surface of the SiO_2 film with a surface roughness of 0.5 nm, indicating a high quality of ALD-grown SiO_2 films. Figure 1(c) shows the leakage current density vs applied voltage for various SiO_2 films (5–20 nm) with an MOS structure. The measured current is tens of picoampere regardless of SiO_2 thickness, corroborating a good insulating SiO_2 film as well as high quality of the SiO_2 film down to 5 nm (the current density at a bias voltage of −3 V, as shown in Table I). A clear hysteresis current–voltage loop is observed under high voltage, indicating a carrier trapping/detrapping process in the SiO_2/Si structure. The corresponding semi-log current–voltage curves are displayed in Fig. 1(d).

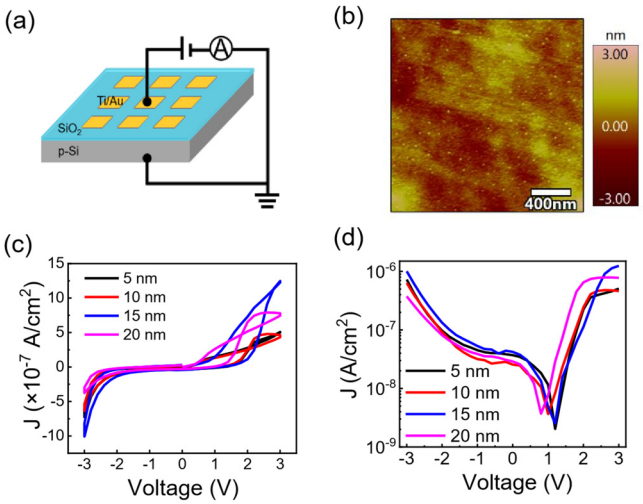

FIG. 1. (a) Schematic diagram of characterization. (b) The typical morphology of a 10 nm SiO_2 film. (c) The current density vs applied voltage (J–V curve) for various thicknesses of SiO_2 heterostructures. (d) The semi-log curve of J–V in (c).

TABLE I. The SiO_2 thickness-dependent extracted parameters including V_{fb}, the current density at −3 V, Q_{ox}, and D_{it}.

Sample (nm)	V_{fb} (V)	J ($\times 10^{-6}$ A cm^{-2})	Q_{ox} ($\times 10^{10}$ cm^{-2})	D_{it} ($\times 10^{12}$ eV^{-1} cm^{-2})
5	−0.90	0.73	2.43	4.46
10	−0.93	0.64	2.42	4.29
15	−0.95	1.01	2.65	2.68
20	−0.87	0.38	2.46	2.30

Conventional capacitance characterization was conducted to extract D_{it} as shown in Fig. 2. The typical $G/\omega - f$ characteristic was measured at a gate voltage ranging from the accumulation region to the depletion region (from −1.2 to −0.4 V) [Figs. 2(a) and 2(b)]. The $G/\omega - f$ curve can be well fitted by an equivalent circuit of the series resistance correction (SRC, R_S) model [the inset of Fig. 2(a)], where R_S is primarily supplied by the substrate.[4,26,27] Then, the interface conductance (G_p) and interface capacitance (C_p) can be well extracted, which can precisely describe the contribution of conductance and capacitance from the SiO_2/Si interface [Fig. 2(c)].

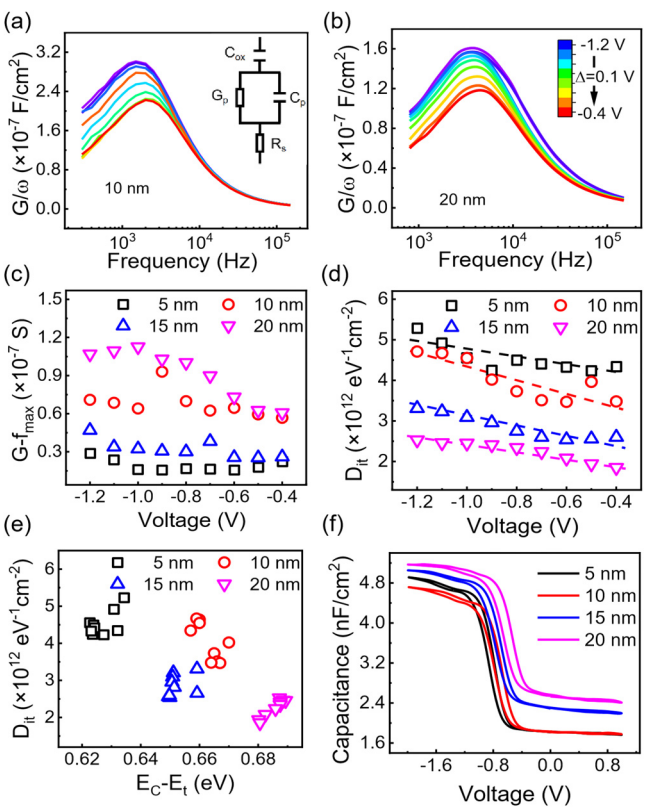

FIG. 2. The typical ratio of ac conductance over angular frequency (G/ω) as a function of frequency (f) under various gate voltages for (a) 10 nm SiO_2 films and (b) 20 nm SiO_2 films. (c) The voltage-dependent peak value from the G–f curve for various SiO_2 thicknesses. (d) The voltage-dependent extracted D_{it}. (e) The relation between the extracted D_{it} and the energy level (E_C–E_t). (f) The capacitance vs voltage curves for various SiO_2 thicknesses.

Generally, a conductance peak appears when sweeping the frequency at a certain voltage, corresponding to the maximum energy loss due to the resonation of interface traps at a given frequency.[27,28] It also reveals the energy level of the interface state related to the Fermi level during the charge trapping process.[29,30] The voltage that drives the maximum peak position shift is always connected to identify the efficiency of the Fermi level movement, which can be used to estimate the interface state.[31,32] Moreover, the maximum peaks show a weak variation with the change of applied voltage, indicating possible interface energy level pinning.[33] Therefore, the interface state can be quantitatively calculated by the following relationship:

$$D_{it} \approx \frac{2.5}{Aq}\left(\frac{Gp}{\omega}\right)_{max}, \tag{2}$$

where G_p/ω, A, and q are the fitted maximum peak value in the $G/\omega - f$ curve, the electrode area, and the element charge, respectively. Clearly, it is with slightly larger D_{it} (4.24–5.23×10^{12} eV^{-1} cm^{-2}) for a thin SiO_2 film (5 nm) as compared to that of a thick SiO_2 film (2.34–3.31×10^{12} eV^{-1} cm^{-2}) [Fig. 2(d)]. This indicates that the increase of the SiO_2 thickness can slightly improve the interface quality. A similar effect was observed in HfO_2 thin films.[34,35] The calculated D_{it} slightly decreases as the carrier changes from the accumulation region to the depletion region, irrespective of SiO_2 thickness, consistent with the weak voltage-dependent peak position. The variation of D_{it} is slightly larger in 5 and 10 nm SiO_2 films compared to that of 15 and 20 nm films.

The voltage can drive the movement of the Fermi level by band filling, which helps us to understand the distribution of interface state density. The D_{it} distribution as a function of energetic position (ΔE) can be roughly determined by the full interface state model,[26,36]

$$\Delta E = E_C - E_t = \frac{k_B T}{q} \times \ln\left(\frac{\sigma v_{th} D_{dos}}{\omega}\right). \tag{3}$$

Here, the energetic position (ΔE) is the energy difference between the interface trap level (E_t) and majority carrier band edges (E_C or E_V). k_B and T are the Boltzmann constant and the temperature, respectively. As for SiO_2, σ, v_{th}, D_{dos}, and ω are the capture cross section of the trap in SiO_2 (1.0×10^{15} cm^{-2}), the average carrier thermal velocity (1.6×10^7 cm s^{-1}), the effective conduction band density of states (2.8×10^{19} cm^{-3}), and the applied angular frequency ($\omega = 2\pi f$), respectively. The extracted ΔE and D_{it} are localized at a small value [shown in Fig. 2(e)], verifying the band pinning effect in the band structure.

Figure 2(f) shows the C–V characteristics of SiO_2/p-Si MOS capacitors measured at 1 MHz; the difference between the theoretically calculated results and the actual measured results is due to the equivalent Rs in the circuit. The equivalent Rs can affect the measured capacitance, resulting in a lowered capacitance as well as the abnormal thickness-dependent capacitance in our result.[34,37,38] Capacitance does not saturate at the accumulation region, indicating

the existence of carrier trapping. A clear hysteresis character is observed, corroborating the interface state in all SiO_2/Si films. Q_{ox} in the oxide layer can be calculated by the following relationship:[31,39–41]

$$Q_{ox} = -C_{max}(V_{fb} + V_{ms})/Aq, \tag{4}$$

where C_{max}, V_{fb}, and V_{ms} are the maximum capacitance at 1 MHz, flatband voltage,[40] and the work function difference between the metal gate (Au) and the semiconductor, respectively. The extracted Q_{ox} is around 2.49×10^{10} cm^{-2} (Table I), which is consistent with previous reports.[42]

Generally, the TD-SHG signal can be used to comprehensively understand the laser-induced electron transport dynamics.[13,18,43] A schematic of laser-induced electron transport/transfer as well as the modulation of the interfacial electric field is shown in Figs. 3(a) and 3(b). At the static state without the laser irradiation, the internal electric field E_{dc} forms due to the presence of the fixed charges near the interface, contributing to the SHG signal at the initial state. After the laser irradiation, a large number of electrons in Si are excited and transferred to the SiO_2 film, leaving the holes to sit at the position. Accordingly, the laser-induced electric field is built due to the laser irradiation, which can enhance/reduce the total electric field. Continuous laser irradiation generates photoexcited carriers that get trapped at the border and oxide trap levels. These trapped electrons dominate the electric field E_{dc}, resulting in a decrease in the absolute electric field E_{dc} and the EFISH intensity. Over time, the photo-excited electrons continue to overcome the interface barrier and get trapped in the oxide or at the oxide surface. These oxide and surface trappings of electrons lead to a rise in the electric field (in the opposite direction). In this case, the TD-SHG can be used to effectively detect the modulation of a competing interfacial electric field between the minimum electric field and laser-induced electric field, which can be correlated to the defects or interface state density in the sample [Figs. 3(c) and 3(d)]. When the 300 mW laser beam irradiates the 10 nm SiO_2/Si sample, the SHG signal monotonically increases with time and it approaches saturation in 5 s as shown in Fig. 3(c), thereby revealing the generation of a time-dependent quasi-static field at the interface. TD-SHG with a low excitation energy of 100 mW shows a decrease in the first second and then it increases with time [Fig. 3(d)]. The minimum value in TD-SHG corresponds to the compensation point between the minimum build-in electric field and the laser-induced electric field. The SHG signal is related to the induced electric field, which can be from interface or bulk defects in the sample. Since the SHG minimum point correlates to the compensation of electric field at the interface, the SHG value at the minimum should correspond to the fixed charges in the SiO_2. Therefore, it seems the SHG value at the minimum point increases with the thickness of the SiO_2 film, corresponding to an increase of the total defects with the film thickness.

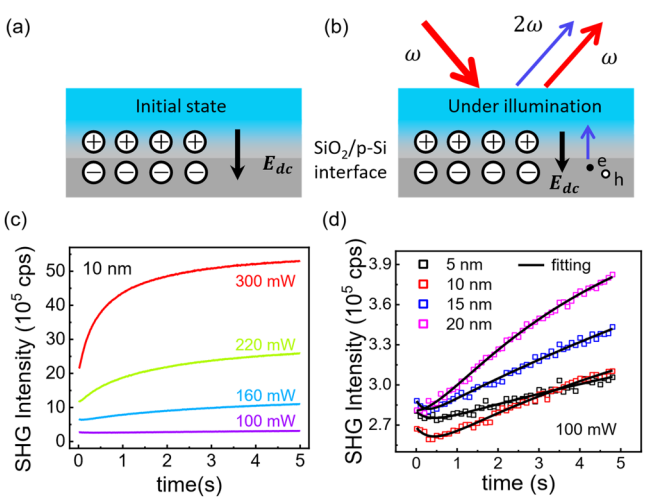

FIG. 3. The schematic figures of the interfacial electric field (a) before laser illumination and (b) after laser illumination. (c) The TD-SHG signals under different laser powers for a typical 10 nm SiO_2 heterostructure. (d) The TD-SHG signal under 100 mW for various SiO_2 thicknesses. The corresponding exponential fittings are shown as solid lines in (d).

The TD-SHG data can be well fitted by the following equation:[10–12]

$$\sqrt{I_{2\omega}(t)} \propto a_0 + a_1\left(1 - e^{-\frac{t}{\tau_1}}\right) + a_2\left(1 - e^{-\frac{t}{\tau_2}}\right), \tag{5}$$

where a_i are constants (independent of each sample, where a_i are constants related to the initial and saturation SHG intensities, and the relative contribution of each type of traps) and τ_i corresponds to the fast (τ_1) and slow (τ_2) trapping process. Here, $I_{2\omega}(t)$ and τ are the intensity of the SHG signal and the time constant associated with the carrier trapping/detrapping process. (Here, we mainly consider the time of slow interface state filling. The time of fast interface state filling is negligibly small, which is out of our consideration.)[44,45] We define $1/\tau$ as the electron trapping rate. The extracted electron trapping rate $1/\tau_2$ linearly increases with the increase in power density as shown in Fig. 4(a), which yields the relation $1/\tau_2 \propto (I_\omega)^n$ with $n = 2.83 \pm 0.29$. This indicates that three-photon absorption is required to excite electrons from the Si valence band (VB) to the SiO_2 conduction band (CB) [Fig. 4(b)], consistent with the laser excitation energy of 1.59 eV (780 nm) and band offset of 4.05–4.60 eV between Si and SiO_2.

The electron trapping at the interface can induce an electric field, which is opposite to the initial electric field. The induced electric field could dominate the interfacial electric field similar to the inversion case under the voltage after sufficient laser irradiation (5 s in this case), which will raise the barrier height at the interface as well as block the electron injection. The maximum increase in the barrier height $\Delta\varphi_{potential}$ due to band bending can be calculated by the following relationship:

$$\Delta\varphi_{potential} = eE_{dc}d_{ox} = \left(e^2 n_e^{\infty} d_{ox}\right)/\varepsilon_{Si}, \tag{6}$$

where n_e^{∞}, d_{ox}, e, and ε_{si} are the surface charge density at the time $t = \infty$, the oxide layer thickness, the electron charge, and the dielectric constant of silicon, respectively. Here, we take a 5 nm Si/SiO_2 sample for example. We used the calculated D_{it} (4.46×10^{12} eV^{-1} cm^{-2}) for n_e^{∞}. Then, the original expression

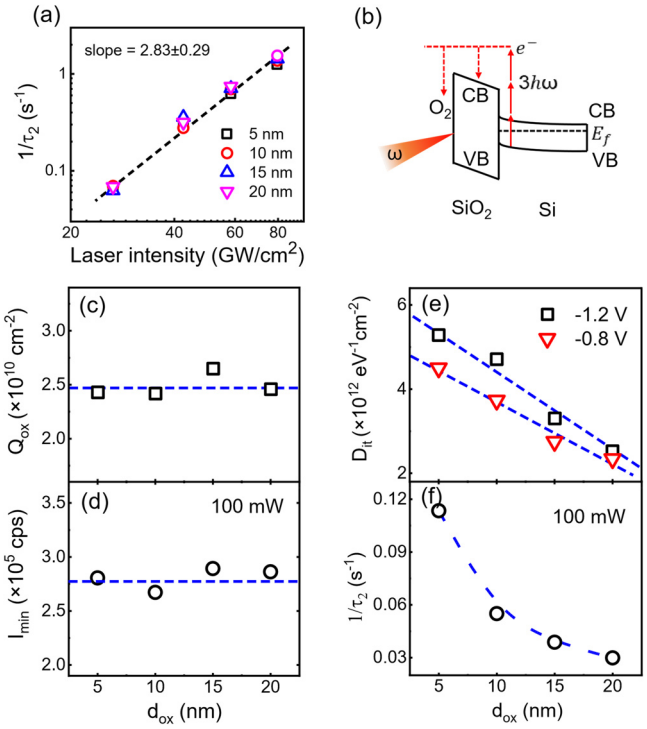

FIG. 4. (a) The extracted trap filling rate vs the laser power density. The solid line is the linear fitting. (b) The corresponding schematic energy diagram of the SiO_2/Si heterostructure. The SiO_2 thickness dependence of (c) the extracted Q_{ox}, (d) the I minimum SHG intensity extracted from TD-SHG under 100 mW, (e) D_{it} at typical −0.8 and −1.2 V, and (f) the extracted trap filling rate under 100 mW.

changes to the relation $\Delta\varphi_{potential} = \left(e^2 d_{ox} \int D_{it} dE\right)/\varepsilon_{Si}$. So, the calculated minimum increase of potential height reaches 0.34 eV for the 5 nm Si/SiO_2 sample.

Finally, a connection between the conventional CV characterization and TD-SHG is established to efficiently understand the surface state, as shown in Figs. 4(c)–4(f). The calculated Q_{ox} is around $2.49 \pm 0.16 \times 10^{10}\,cm^{-2}$, which is almost independent of SiO_2 thickness. In TD-SHG, the minimum data point of SHG $2.71 \pm 0.15 \times 10^5$ cps under 100 mW is dominantly attributed to fixed charges in the SiO_2 layer, considering no contribution from the interfacial electric field due to the compensation between the minimum electric field and the laser-induced electric field at the interface. Q_{ox} is closely related to the sample preparation process and the crystal direction, which is independent of the sample thickness. Correspondingly, the intensity of minimum SHG data may be used to qualitatively catch Q_{ox} in the oxide layer. The typical D_{it} under −0.8 and −1.2 V are displayed in Fig. 4(e), which are extracted by the conductance method. D_{it} is almost linearly decreasing with the increase in oxide thickness, which is with a slight slope deviation with different gate voltages. The linear relation may be related to a high-quality interface for the thick SiO_2 film and the low-quality interface with a high density of dangling bonds or defects in the thin SiO_2 film, which may originate from the sample preparation process. As for τ extracted from Eq. (5), it is connected to the carrier trapping/detrapping at the interface, which is closely related to D_{it}. Namely, the high D_{it} can result in a fast electron trapping rate $1/\tau_2$. Here, the extracted $1/\tau_2$, ranging from 0.0299 to $0.1134\,s^{-1}$ (laser power 100 mW), linearly increases with the increase inf the oxide layer thickness. It reveals that D_{it} may be linearly related to the extracted $1/\tau_2$ with the SiO_2 thickness ranging from 5 to 20 nm, indicating that the thin SiO_2 is with high D_{it} and a fast electron trapping rate $1/\tau_2$. It is noted that the linear relation may vary with a wide range of the SiO_2 thickness, which needs to be further investigated. All the data indicate that TD-SHG is a simple and fast method for extracting the important semiconductor parameters such as Q_{ox}, D_{it} etc., which may facilitate in-line semiconductor monitoring.

IV. CONCLUSION

In summary, this work utilizes the time-dependent second harmonic generation method to characterize the interface state density and fixed charge density of the SiO_2/Si interface, which is compared with the traditional conductance method. We found that a minimum signal under a low laser power in EFISH is mainly related to Q_{ox}, while the time evolution of SHG corresponds to D_{it}. The extracted Q_{ox} measured by the conventional high-frequency C–V method is around $2.49 \times 10^{10}\,cm^{-2}$, regardless of the SiO_2 thickness, which is closely related to the constant SHG intensity at the minimum of TD-SHG. In addition, the static electric field at the interface is estimated by the C–V method. The extracted D_{it} linearly decreases with the SiO_2 thickness, which is related to the linear decrease of the extracted $1/\tau_2$ from TD-SHG. Accordingly, as a qualitative, sensitive, non-contact, and fast technique, TD-SHG could serve as a viable alternative for evaluating semiconductor parameters, potentially streamlining semiconductor metrology processes.

ACKNOWLEDGMENTS

This work was supported by the National Natural Science Foundation of China (NNSFC) (Grant No. 12104005), the Scientific Research Foundation of the Higher Education Institutions for Distinguished Young Scholars in Anhui Province (Grant No. 2022AH020012), and the Innovation Project for Overseas Researcher in Anhui Province (Grant No. 2022LCX004). This work was also supported by Shanghai Aspiring Semiconductor Equipment Co., Ltd and Aspiring Semiconductor (Beijing) Co., Ltd. We are thankful for the use of the micro- and nano-scale clean room at the AHU Quantum Materials Center for facilitating the experimental work. This work was also partially supported by the facilities at Center of Free Electron Laser & and High Magnetic Field (FEL&HMF) in Anhui University.

AUTHOR DECLARATIONS

Conflict of Interest

The authors have no conflicts to disclose.

Author Contributions

Libo Zhang: Formal analysis (equal); Investigation (equal); Visualization (equal); Writing – original draft (equal). **Li Ye:** Investigation (equal); Visualization (equal). **Weiwei Zhao:** Formal analysis (equal); Investigation (equal); Resources (equal). **Chongji Huang:** Formal analysis (equal); Investigation (equal). **Tao Li:** Investigation (supporting). **Tai Min:** Investigation (equal). **Jinbo Yang:** Formal analysis (equal); Investigation (equal). **Mingliang Tian:** Conceptualization (equal); Supervision (equal); Writing – review & editing (equal). **Xuegang Chen:** Conceptualization (equal); Formal analysis (equal); Funding acquisition (equal); Supervision (equal); Writing – original draft (equal); Writing – review & editing (equal).

DATA AVAILABILITY

The data that support the findings of this study are available from the corresponding author upon reasonable request.

REFERENCES

[1] A. Aktağ, A. Mutale, and E. Yılmaz, J. Mater. Sci. Mater. Electron. **31**, 9044 (2020).
[2] N. Yoshida, E. Waki, M. Arai, K. Yamasaki, J.-H. Han, M. Takenaka, and S. Takagi, Thin Solid Films **557**, 237 (2014).
[3] A. Tataroğlu and Ş. Altındal, Microelectron. Eng. **85**, 2256 (2008).
[4] S. Abubakar and E. Yilmaz, Microelectron. Eng. **232**, 111409 (2020).
[5] P. Zhao, A. Khosravi, A. Azcatl, P. Bolshakov, G. Mirabelli, E. Caruso, C. L. Hinkle, P. K. Hurley, R. M. Wallace, and C. D. Young, 2D Mater. **5**, 031002 (2018).
[6] Z. Jian, S. Mohanty, and E. Ahmadi, Appl. Phys. Lett. **116**, 242105 (2020).
[7] W. Liu, I. Sayed, C. Gupta, H. Li, S. Keller, and U. Mishra, Appl. Phys. Lett. **116**, 022104 (2020).
[8] N. Novkovski, J. Phys. Commun. **1**, 035006 (2017).
[9] J. L. Fiore, V. V. Fomenko, D. Bodlaki, and E. Borguet, Appl. Phys. Lett. **98**, 041905 (2011).
[10] T.-Y. Yen, M.-T. Shih, L.-F. Song, K.-M. Hung, and K.-Y. Lo, Surf. Interfaces **41**, 103236 (2023).
[11] H. Park, J. Qi, Y. Xu, K. Varga, S. M. Weiss, B. R. Rogers, G. Lüpke, and N. Tolk, Appl. Phys. Lett. **95**, 062102 (2009).
[12] D. Damianos, G. Vitrant, A. Kaminski-Cachopo, D. Blanc-Pelissier, G. Ghibaudo, M. Lei, J. Changala, A. Bouchard, X. Mescot, M. Gri, S. Cristoloveanu, and I. Ionica, J. Appl. Phys. **124**, 125309 (2018).
[13] Z. Marka, R. Pasternak, S. N. Rashkeev, Y. Jiang, S. T. Pantelides, N. H. Tolk, P. K. Roy, and J. Kozub, Phys. Rev. B **67**, 045302 (2003).
[14] M. Lei, J. Price, and M. C. Downer, Appl. Phys. Lett. **96**, 241105 (2010).
[15] D. Li, X. Huang, Q. Wu, L. Zhang, Y. Lu, and X. Hong, Adv. Mater. **35**, 2208825 (2023).
[16] J. Qin, F. Huang, X. Li, L. Deng, T. Kang, A. Markov, F. Yue, Y. Chen, X. Wen, S. Liu, Q. Xiong, S. Semin, T. Rasing, D. Modotto, R. Morandotti, J. Xu, H. Duan, and L. Bi, ACS Nano **13**, 1213 (2019).
[17] J. Nordlander, G. De Luca, N. Strkalj, M. Fiebig, and M. Trassin, Surf. Sci. **8**, 570 (2018).
[18] B. Jun, Y. V. White, R. D. Schrimpf, D. M. Fleetwood, F. Brunier, N. Bresson, S. Cristoloveanu, and N. H. Tolk, Appl. Phys. Lett. **85**, 3095 (2004).
[19] J. Mihaychuk, N. Shamir, and H. van Driel, Phys. Rev. B **59**, 2164 (1999).
[20] N. Shamir, J. Mihaychuk, and H. van Driel, J. Appl. Phys. **88**, 896 (2000).
[21] O. A. Aktsipetrov, A. A. Fedyanin, E. D. Mishina, A. N. Rubtsov, C. W. van Hasselt, M. A. C. Devillers, and B. Rasing, Phys. Rev. B **54**, 1825 (1996).
[22] J. R. Weber, A. Janotti, and C. G. Van de Walle, J. Appl. Phys. **109**, 033715 (2011).
[23] J. Bloch, J. G. Mihaychuk, and H. M. van Driel, Phys. Rev. Lett. **77**, 920 (1996).
[24] T. Scheidt, E. G. Rohwer, P. Neethling, H. M. von Bergmann, and H. Stafast, J. Appl. Phys. **104**, 083712 (2008).
[25] J. G. Mihaychuk, J. Bloch, Y. Liu, and H. M. van Driel, Opt. Lett. **20**, 2063 (1995).
[26] W. Cai, M. Takenaka, and S. Takagi, J. Appl. Phys. **115**, 094509 (2014).
[27] W. Zhu, T. Low, Y. H. Lee, H. Wang, D. B. Farmer, J. Kong, F. Xia, and P. Avouris, Nat. Commun. **5**, 3087 (2014).
[28] A. Ghosh, R. Lahiri, S. M. M. Dhar Dwivedi, and A. Mondal, J. Appl. Phys. **128**, 095704 (2020).
[29] A. Turut, A. Karabulut, K. Ejderha, and N. Bıyıklı, Mater. Sci. Semicond. Process. **39**, 400 (2015).
[30] X. Song, X. Liang, J. Min, J. Zhang, S. Li, P. Qiu, C. Feng, C. Xie, L. Dai, J. Chen, Y. Shen, and L. Wang, Mater. Sci. Semicond. Process. **148**, 106809 (2022).
[31] L. Qiao, G. He, L. Hao, J. Lu, Q. Gao, M. Zhang, and Z. Fang, IEEE Electron Device Lett. **68**, 2899 (2021).
[32] S. Li, J. Luo, and T. Ye, ECS J. Solid State Sci. Technol. **12**, 053006 (2023).
[33] M. Ishfaq, M. R. Khan, A. Ali, S. Bhardwaj, C. Cepek, and A. S. Bhatti, Mater. Sci. Semicond. Process. **63**, 107 (2017).
[34] S. Dueñas, H. Castán, H. García, J. Barbolla, K. Kukli, J. Aarik, and A. Aidla, Semicond. Sci. Technol. **19**, 1141 (2004).
[35] K. B. Jinesh, J. L. van Hemmen, M. C. M. van de Sanden, F. Roozeboom, J. H. Klootwijk, W. F. A. Besling, and W. M. M. Kessels, J. Electrochem. Soc. **158**, G21 (2011).
[36] T. Haffner, M. A. Mahjoub, S. Labau, J. Aubin, J. M. Hartmann, G. Ghibaudo, S. David, B. Pelissier, F. Bassani, and B. Salem, Appl. Phys. Lett. **115**, 171601 (2019).
[37] K. Zeng and U. Singisetti, Appl. Phys. Lett. **111**, 122108 (2017).
[38] E. Verrelli, D. Tsoukalas, and D. Kouvatsos, Phys. Status Solidi C **5**, 3720 (2008).
[39] L. Hao, G. He, G. Zheng, Q. Gao, L. Qiao, and Z. Fang, ACS Appl. Electron. Mater. **3**, 872 (2021).
[40] A. Mutale, S. C. Deevi, and E. Yilmaz, J. Alloys Compd. **863**, 158718 (2021).
[41] P. Samanta, J. Vac. Sci. Technol. B **37**, 062204 (2019).
[42] G. H. Tsau, A. Sher, M. Madou, J. A. Wilson, V. A. Cotton, and C. E. Jones, J. Appl. Phys. **59**, 1238 (1986).
[43] T.-Y. Yen, Y.-H. Huang, M.-T. Shih, W.-T. Chen, K.-M. Hung, and K.-Y. Lo, Surf. Interfaces **36**, 102541 (2023).
[44] B. Mallick, D. Saha, A. Datta, and S. Ganguly, ACS Appl. Mater. Interfaces **15**, 38888 (2023).
[45] B. Mallick, D. Saha, A. Datta, and S. Ganguly, Solid State Electron. **199**, 108502 (2023).